Ceramics International 45 (2019) 17758–17766

Contents lists available at ScienceDirect

Ceramics International

journal homepage: www.elsevier.com/locate/ceramint

# Characterizations of P(VDF-HFP)-$BaTiO_3$ nanocomposite films fabricated by a spin-coating process

Xu Lu[a,*], Xiaowan Zou[a], Jialiang Shen[b], Li Jin[c], Fuxue Yan[a], Gaoyang Zhao[a], Lin Zhang[c], Z.-Y. Cheng[b,**]

[a] Laboratory of Functional Films, School of Materials Science and Engineering, Xi'an University of Technology, Xi'an, 710048, China
[b] Materials Research and Education Center, Auburn University, Auburn, AL, 36849, USA
[c] Electronic Materials Research Laboratory, Key Laboratory of the Ministry of Education & International Center for Dielectric Research, School of Electronic and Information Engineering, Xi'an Jiaotong University, Xi'an, 710049, China

ARTICLE INFO

*Keywords:*
Nanocomposite
P(VDF-HFP)
$BaTiO_3$
Dielectric
Molecular mobility

ABSTRACT

In this work, free-standing and flexible polymer-ceramic nanocomposite films were fabricated by a spin-coating process using poly(vinylidene fluoride-co-hexafluoropropylene) [P(VDF-HFP)] as matrix and $BaTiO_3$ (BTO) nanoparticles as filler. The relationships between the properties and compositions were systematically investigated. It is experimentally found that the crystallinity and the size of crystals of the P(VDF-HFP) matrix decreases with increasing BTO content. The dielectric responses of the polymer used as matrix were determined by four dielectric processes. Both the temperature and frequency dependences of the dielectric responses obtained in the composite films are mainly determined by the polymer matrix, and the influences of the ceramic filler on the four dielectric processes of the polymer matrix were discussed.

## 1. Introduction

As is well known, dielectric capacitors are widely used in the pulsed-power systems, in which the stored energy needs to be charged/discharged over a short time period and in a controlled manner. Dielectric materials with a high dielectric constant ($\varepsilon_r$), a low dielectric loss (tan$\delta$) and a high electric breakdown strength ($E_b$) are demanded. Both ceramics and polymers have been extensively studied and widely used as dielectric materials in energy-storage capacitors.

Ceramics, especially lead-free perovskite ceramics, are considered as one of the most promising materials for the development of the pulsed-power systems due to their high $\varepsilon_r$ [1]. In recent years, a series of dielectric ceramics, such as $BaTiO_3$-based [2], (Ba/Sr)$TiO_3$-based [3], $AgNbO_3$-based [4], (K/Na)$NbO_3$-based [5], (Na/Bi)$TiO_3$-based [6], and $NaNbO_3$-based [7] ceramics, have been developed for the energy-storage applications. Although great progress has been made, the applications of dielectric ceramics are still limited by their low $E_b$, high weight, high processing temperature, etc.

Polymers with quite high $E_b$ are also widely used as dielectric materials in energy-storage capacitors. In addition, polymers are flexible, light in weight, and can be processed at low temperature. Polymers, such as polypropylene (PP), polyester (PET), polycarbonate (PC), polyphenylene-sulfide (PPS), have been widely used as flexible dielectric films, but the low dielectric constant (~2–3) limits their applications [8]. Due to the contribution of the high density of dipoles in the polar polymers to their dielectric responses [9], poly(vinylidene fluoride) (PVDF) and its copolymers/terpolymers, such as poly(vinylidene fluoride-co-trifluoroethylene) [P(VDF-TrFE)] [10], poly(vinylidene fluoride-co-chlorotrifluoroethylene) [P(VDF-CTFE)] [11], and poly(vinylidene fluoride-co-hexafluoropropylene) [P(VDF-HFP)] [12], poly (vinylidene fluoride-co-trifluoroethylene-co-chlorofluoroethylene) [P(VDF-TrFE-CFE)] [13], have attracted a lot of attentions owing to their high $\varepsilon_r$ (~10) [14–16].

Composite approach has been used to enhance the $\varepsilon_r$ of polymers by introducing high-$\varepsilon_r$ ceramic particles into polymer matrix, i.e. polymer-ceramic composites [17–20]. Polymer-ceramic composites take typical advantages of the good flexibility of polymers and the high $\varepsilon_r$ of ceramics. In addition, polymer-ceramic composites are light in weight, and can be fabricated through low temperature processes. Regarding the matrix, PVDF based polymers have been extensively utilized due to their good flexibility and relatively high $\varepsilon_r$. Regarding the filler, ceramic nanoparticles, such as $BaTiO_3$ [21–25], $CaCu_3Ti_4O_{12}$ [26–30], (Ba/Sr)$TiO_3$ [31–34], have been widely used due to their high $\varepsilon_r$.

Regarding the fabrication processes, the compatibility between the

* Corresponding author.
** Corresponding author.
*E-mail addresses:* lux@xaut.edu.cn (X. Lu), chengzh@eng.auburn.edu (Z.-Y. Cheng).

https://doi.org/10.1016/j.ceramint.2019.05.346
Received 21 March 2019; Received in revised form 28 May 2019; Accepted 30 May 2019
Available online 01 June 2019

polymer matrix and the ceramic particles and the uniformity in microstructure are critical [35–37]. That is, the properties of the polymer-ceramic composite films depend, to a great extent, on the fabrication processes. Melting blend process and solvent-based processes are widely utilized in the fabrication and study of the polymer-ceramic composites. The melting blend process is carried out above the melting temperature ($T_m$) of the polymers, and is normally used to fabricate composites with insoluble polymers as matrix, such as PP and PE [38–40]. The solvent-based processes are the most popular methods in the investigation of the polymer-ceramic composites. In the solvent-based processes, ceramic particles are dispersed in a polymer solution, and composites can be obtained by evaporating the solvent. Solution-casting process is one of the popular methods in the development of polymer-ceramic composite films [18,22,24,26,27,29,31–34]. However, due to the aggregation of the filler particles caused by gravity during the solvent evaporation, the composite films fabricated by solution-casting process normally show poor uniformity. To obtain better microstructure uniformity, a stack of composite films fabricated by solution-casting process could be hot-pressed into one layer [18,29,31,33,41–43]. In our previous works, a spin-coating process using thick polymer solution has been developed in the fabrication and study of the polymer-ceramic nanocomposite films [44–46]. Owing to the enhanced stability of the polymer-ceramic-solvent suspension and the fast solidification, excellent microstructure uniformity can be obtained in the nanocomposite films fabricated by the spin-coating process. Besides the sphere-like ceramic nanoparticles, ceramic nanofibers [47–54], core-shell nanoparticles [52,54–62], etc., have been widely used in the fabrication and investigation of the polymer-ceramic nanocomposite films. The interface between the matrix and the filler particles is also critical for the performances of the composites and could been improved using kinds of coupling agents or chemical treating methods [47,48,51,63–69].

From the application point of view, most of the recent reports are mainly focused on the enhancements of the dielectric constant ($\varepsilon_r$) and electric breakdown strength ($E_b$) of the polymer-ceramic composites, which are directly related to the energy-storage performances. It is well known that a composite is a material made from two or more constituents with significantly different physical or chemical properties, and that the interaction between those constituents is critical to the properties. Although a lot of efforts have been made in the development of polymer-ceramic composites, it has to be noted that, the interaction between the ceramic nanoparticles and the polymer matrix and its influences on the evolution of the molecular mobility of the polymer matrix are still not clear, which are meaningful for the understanding of ceramic-polymer composites and needs to be further studied.

In this work, polymer-ceramic nanocomposite films were fabricated using a spin-coating process and systematically characterized to understand the relationships between the properties and compositions, especially the influences of the ceramic nanoparticles on the relaxation processes related to the evolution of the polymer molecular mobility. P(VDF-HFP) with 15 wt% of HFP was used as the matrix due to its excellent flexibility and good dielectric properties, and sphere-like BTO nanoparticles (about 60 nm in diameter) were used as the filler due to its high $\varepsilon_r$ and relatively low tan$\delta$. Large pieces of P(VDF-HFP)-BTO nanocomposites films were fabricated in this work, and their microstructure is dense and uniform. Both the $\varepsilon_r$ and tan$\delta$ of the P(VDF-HFP)-BTO films were systemically examined at different temperatures and frequencies. It is found that the dielectric responses of the P(VDF-HFP)-BTO films are determined by the polymer as matrix and affected by the filler content.

## 2. Experiments

### 2.1. Materials and chemicals

P(VDF-HFP) with 15 wt% of HFP was provided by PolyK. $BaTiO_3$ (BTO) nanoparticles with a nominal diameter of 60 nm and with a specific surface area (SSA) of 15.00–17.60 $m^2/g$ were provided by Sinocera. The densities of P(VDF-HFP) pellets and BTO nanoparticles are 1.78 $g/cm^3$ and 6.02 $g/cm^3$ respectively. N, N-dimethyl formamide (DMF) was purchased from Sinopharm. Glass plates (50 mm × 50 mm × 0.8 mm) were purchased from Guluoglass. All the materials and chemicals were used as received.

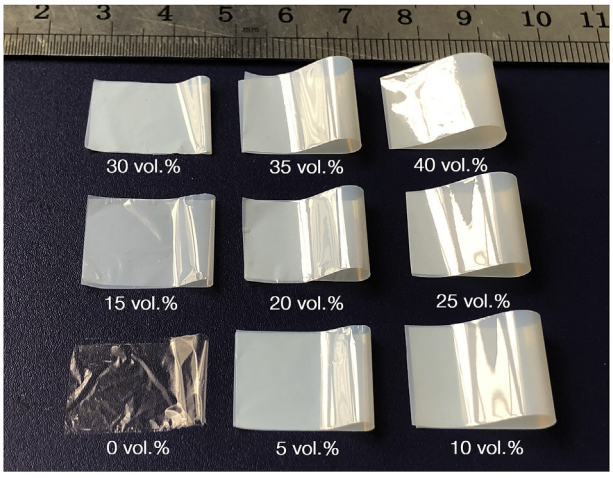


**Fig. 1.** Freestanding, flexible, translucent P(VDF-HFP)-BTO nanocomposite films fabricated by a spin-coating process.

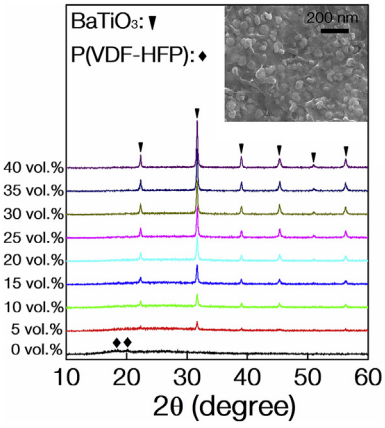


**Fig. 2.** XRD patterns of the P(VDF-HFP)-BTO nanocomposite films. The inset is a typical fracture SEM image of the P(VDF-HFP)-*20*BTO film.

### 2.2. Fabrication of P(VDF-HFP)-BTO films

A series of the (1-*x*)P(VDF-HFP)-*x*BTO films ($x$ = 0, 5, 10, 15, 20, 25, 30, 35, 40 vol%), abbreviated as P(VDF-HFP)-*x*BTO, were fabricated. The typical procedure for fabricating the P(VDF-HFP)-BTO films was operated as follows: Firstly, based on the composition, specific amounts of the P(VDF-HFP) pellets and the BTO nanoparticles were added in DMF and the mixture was fully homogenized by magnetic stirring and ultrasonication. Secondly, the P(VDF-HFP)-BTO-DMF suspension was coated on the pre-cleaned glass plates by a spin-coater (KW-4A, Chemat Technology Inc, Peking, China), and then solidified at 80 °C for about 1 h in an drying oven. After that, the films were stripped off from the glass plates in DI water. Finally, the free-standing P(VDF-HFP)-BTO films were annealed at 140 °C for about 24 h. The pure P(VDF-HFP) film was fabricated by a similar procedure by using a P(VDF-HFP)-DMF solution. Here the thicknesses of all the annealed films are around 5–7 μm.

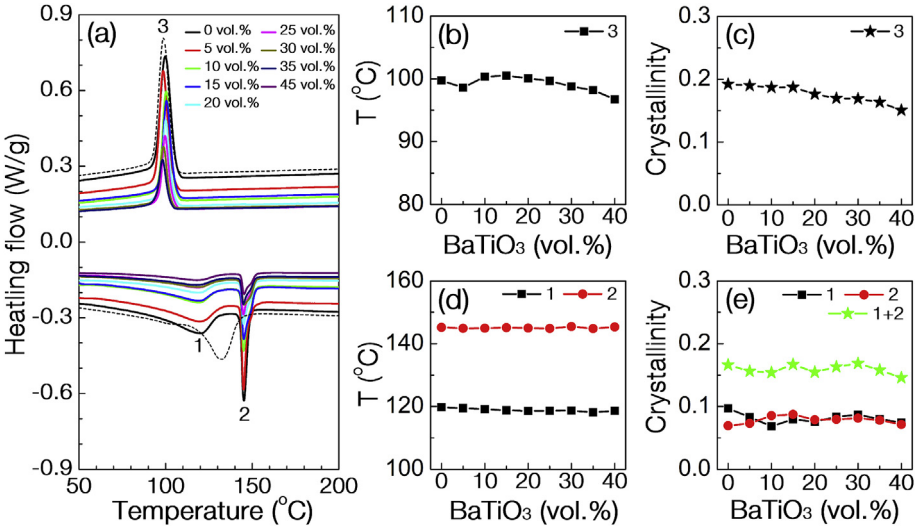


**Fig. 3.** (a) The DSC heating/cooling curves of the P(VDF-HFP)-BTO nanocomposite films. (b) The peak temperature of the cooling curves; (c) the crystallinity calculated from the cooling curves. (d) The peak temperatures of the heating curves; (e) the crystallinity calculated from the heating curves.

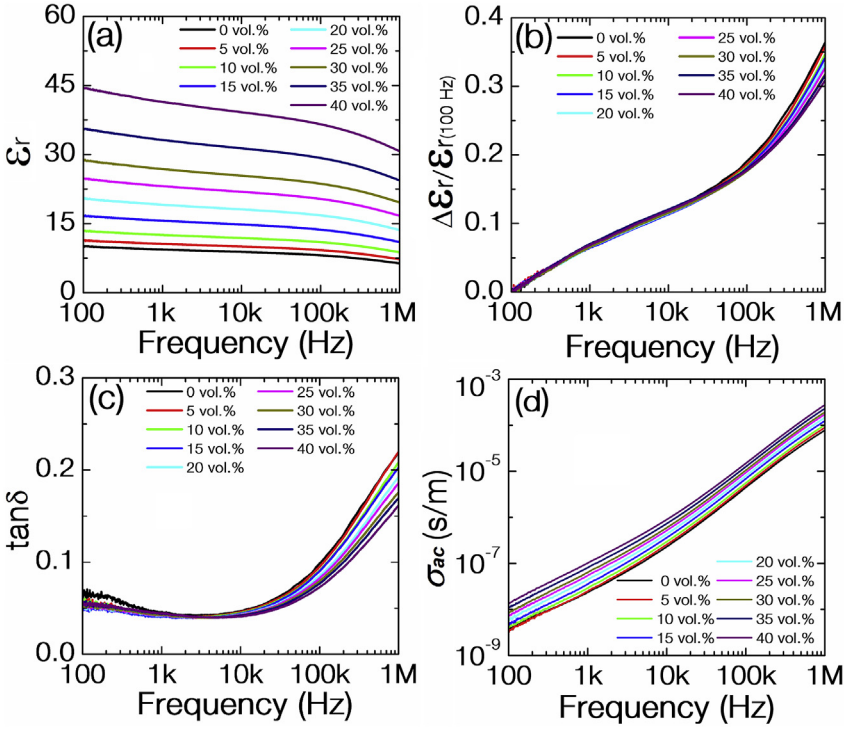


**Fig. 4.** The (a) $\varepsilon_r$, (b) $\Delta\varepsilon_{r/\varepsilon_{r(100\,Hz)}}$, (c) tan$\delta$, and (d) $\sigma_{ac}$ as a function of frequency of the P(VDF-HFP)-BTO nanocomposite films.

### 2.3. Characterizations

The fracture morphologies of the P(VDF-HFP)-BTO films were observed by a field emission scanning electron microscope (JSM-7000F JEOL, Tokyo, Japan). Before that, the nanocomposite films were fractured in liquid nitrogen. The X-ray diffraction (XRD) patterns of all the P(VDF-HFP)-BTO films were examined by an X-ray diffractometer (PANalytical, Cambridge, UK). The differential scanning calorimetry (DSC) was measured by an analyzer (DSC 250, TA Instruments, DE, US) in a temperature range from 50 °C to 200 °C in a nitrogen atmosphere with a heating/cooling rate of 10 °C/min. For the electrical measurements, the films were coated with gold electrodes (3 mm in diameter) on the both sides by a gold coater (JFC-1600, JEOL, Tokyo, Japan). The weak-field (500 mV) dielectric properties were measured by a precision impedance analyzer (4294A, Agilent, CA, USA) in a frequency range from 100 Hz to 1 MHz at room temperature. The temperature dependences of dielectric properties were measured by a precision impedance analyzer (4980, Agilent, CA, USA) in a temperature range from -80 °C to 160 °C under five selected frequencies (100 Hz, 1 kHz, 10 kHz, 100 kHz, and 1 MHz) with a cooling rate of 10 °C/min, during which the samples were placed in a heating & freezing stage (TP94, Linkam, Surrey, UK). The polarization-electric field (*P-E*) loops and corresponding current-electric field (*I-E*) curves were measured at 100 Hz and at room temperature using a commercial ferroelectric testing system (TF analyzer 2000, aixACCT, Aachen, Germany).

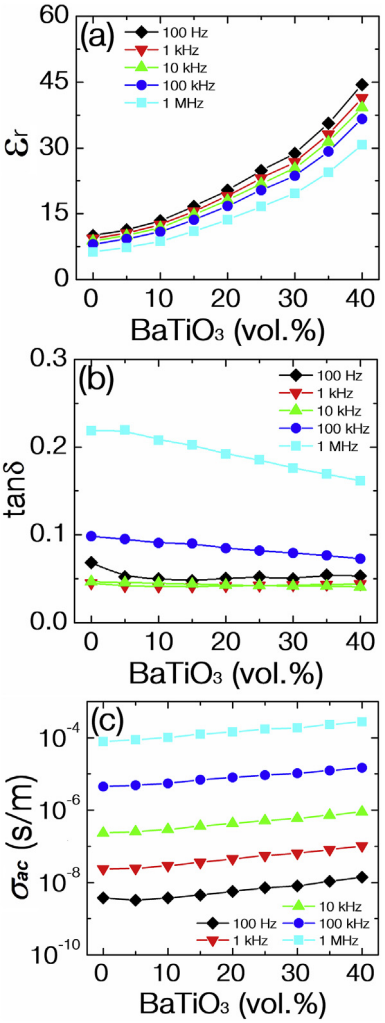


**Fig. 5.** The (a) $\varepsilon_r$, (b) tan$\delta$, and (c) $\sigma_{ac}$ as a function of the BTO content of the P(VDF-HFP)-BTO nanocomposite films.

## 3. Results and discussions

A photo of the P(VDF-HFP)-BTO films fabricated in this work is given in Fig. 1. It is clear that the pure P(VDF-HFP) film is transparent and quite soft owing to its low glass-transition temperature ($T_g$) and low crystallinity. The $T_g$ of P(VDF-HFP) is about -40 °C, above which the P(VDF-HFP) is viscoelastic. Owing to the increasing content of HFP in this copolymer, the crystallinity decreases and the elastic modulus of P(VDF-HFP) can be much smaller than PVDF. It was reported that, compared with PVDF, the elastic modulus of the P(VDF-HFP) with 15 wt% of HFP is about four times smaller [70]. All these suggest that P(VDF-HFP) is a highly soft and very flexible material, which is highly desirable as the matrix for the development of polymer-ceramic composites. All the P(VDF-HFP)-BTO films fabricated here are translucent and of good flexibility. As is well known, for the composite films, the transparency and flexibility can reflect the macro/micro uniformity. That is, the P(VDF-HFP)-BTO films are quite uniform in microstructure with BTO nanoparticles homogeneously dispersed in P(VDF-HFP) matrix. Using the spin-coating process here, large pieces of the nanocomposite films (as large as the glass plates used) could be fabricated.

The XRD patterns of the P(VDF-HFP)-BTO films are given in Fig. 2. For the pure P(VDF-HFP) film, the observed diffraction peaks at 18.4° and 20.3° can be assigned to the α phase and β phase respectively, which indicates that the pure P(VDF-HFP) film is semi-crystalline [50]. There is no obvious peak of P(VDF-HFP) in the XRD patterns of the nanocomposites films, which might reveal the lower crystallinity of the P(VDF-HFP) in the nanocomposite films than the pure P(VDF-HFP) film. The diffraction peaks observed in the nanocomposite films, whose intensities increase with increasing BTO content, are associated with the perovskite structure of the BTO nanoparticles. As an example, a topical fracture SEM image of the P(VDF-HFP)-*20*BTO film is given in the inset of Fig. 2. It is clear that the composite was constructed with BTO nanoparticles dispersed in P(VDF-HFP) matrix. Besides the advantages of the spin-coating process, the excellent microstructure uniformity might also be attributed to a high density of hydroxyl on the surface of the BTO nanoparticles fabricated by hydro-thermal method. That is, for the BTO nanoparticles used as filler, surface-treating process is not requisite to obtain good microstructure uniformity, which leads to the simplification of the fabrication process of polymer-ceramic composite films [71].

To understand the influences of the BTO content on the P(VDF-HFP) matrix, DSC curves of the P(VDF-HFP)-BTO films during the first heating/cooling cycle are given in Fig. 3(a). It is clear that all the curves of the nanocomposite films shown a similar behavior as that of the pure P(VDF-HFP) film. It can be observed that there are two endothermic peaks in the heating curves. The double endothermic peaks were usually reported in the DSC curves of semi-crystalline polymers, and have been attributed to either the melting of two initially coexisting crystal phases or the imperfection of crystallization [72]. Using the pure P(VDF-HFP) film as an example, it is experimentally found that the two endothermic peaks merged into one peak in the second heating cycle, which demonstrates that the imperfect crystallization regions can recrystallize at a higher temperature above the annealing temperature (140 °C) used in this work, as shown in the dash lines in Fig. 3(a). So, it is likely to be the imperfection of crystallization rather than the different crystal phases that determines the melting endotherms in the first heating cycles. There is only one exothermic peak can be observed in the cooling curves, which is associated with the recrystallization of the P(VDF-HFP).

From the data shown in Fig. 3(d), it is found that the temperatures of the two endothermic peaks slightly change with BTO content. Regarding the recrystallization temperature of the polymer matrix, as shown in Fig. 3(b), it observed in the P(VDF-HFP)-*5*BTO film is lower than that of the pure P(VDF-HFP) film, while it, then, increases with increasing BTO content from 5 vol% to 15 vol%, and decreases with further increasing BTO content from 20 vol% to 40 vol%. The recrystallization temperature of the pure P(VDF-HFP) film is 99.7 °C, and the recrystallization temperatures of the P(VDF-HFP) in the composite films with increasing BTO content from 5 vol% to 40 vol% are 98.6 °C, 100.4 °C, 100.5 °C, 100.1 °C, 99.7 °C, 98.8 °C, 98.2 °C and 96.7 °C, respectively. That is, there is a clear influence of the BTO filler on the recrystallization process of the P(VDF-HFP) matrix.

As is well known, during the recrystallization of the polymer matrix, the filler particles can act as either nucleating agents or physical barriers [73–75]. That is, the interface in the composite films increases with increasing content of the ceramic nanoparticles, which could benefit the nucleation of the polymer matrix and leads to a high crystallinity; on the other hand, the recrystallization process may also be slowed down by the BTO nanoparticles, which leads to a lower crystallinity. The effect of the BTO content on the crystallinity of the polymer matrix was analyzed by calculating the melting/crystalline enthalpy normalized to the mass fraction of the polymer matrix in the nanocomposite films in accordance with the relation [76]:

$$\chi = \frac{\Delta H}{\Delta H_0 \times \phi} \times 100\% \quad (1)$$

where $\Delta H$ is the melting/crystalline enthalpy of the P(VDF-HFP)-BTO films; $\Delta H_0$ is the melting enthalpy of pure P(VDF-HFP) with a crystallinity of 100% (104.7 J/g) [73]; $\phi$ is the mass fraction of the P(VDF-HFP) in the P(VDF-HFP)-BTO films.

The crystallinities calculated from the heating/cooling curves of all

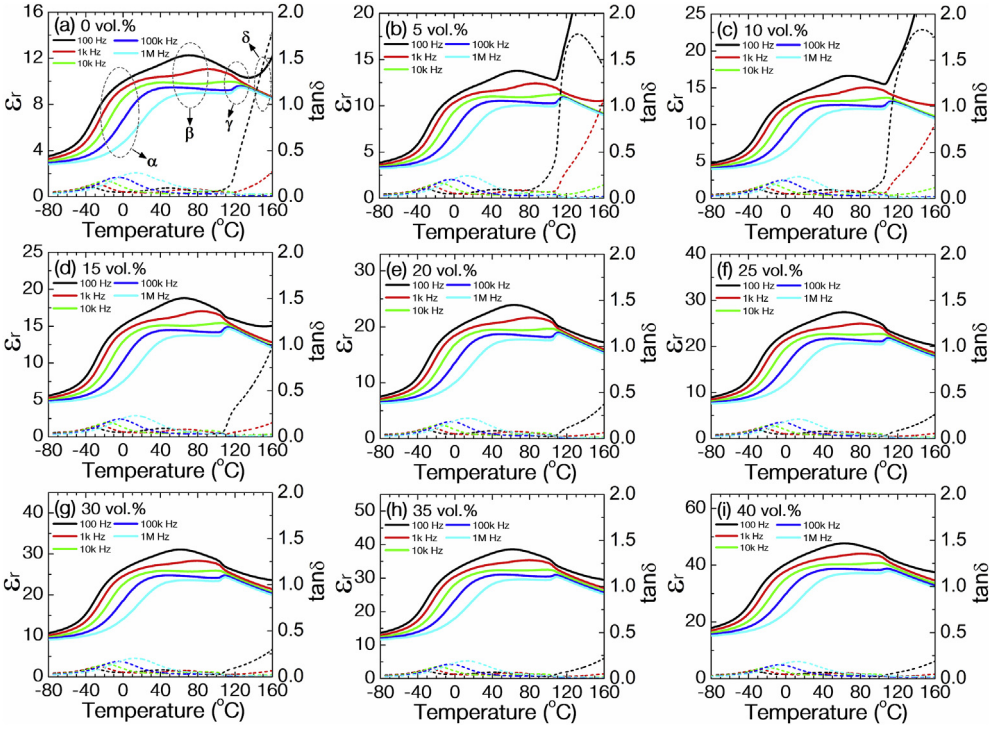


**Fig. 6.** The $\varepsilon_r$ and tan$\delta$ at selected frequencies (100 Hz, 1 kHz, 10 kHz, 100 kHz and 1 MHz) as a function of temperature of the P(VDF-HFP)-BTO nanocomposite films.

the P(VDF-HFP)-BTO films are plotted in Fig. 3(e) and (c) respectively. Based on the heating curves, the total crystallinity value (summed value of the peak 1 and peak 2) of all the films is around 14.6%–16.7% and the variation trend is not very clear. Based on the cooling curves, the crystallinity value clearly decreases with increasing BTO content. The crystallinity value of the P(VDF-HFP) in the nanocomposite films with increasing BTO content from 0 vol% to 40 vol% are 19.2%, 19.0%, 18.7%, 18.7%, 17.6%, 17.0%, 16.9%, 16.3%, and 15.1%, respectively. It can be seen that even with 40 vol% of BTO in the nanocomposite film, the P(VDF-HFP) matrix is still semi-crystalline. These also indicate that the deficiency of P(VDF-HFP) peaks in the XRD patterns of the nanocomposite films might also be attributed to the fact that the size of polymer crystals significantly decreases with increasing BTO content.

The weak-field dielectric spectra of the P(VDF-HFP)-BTO films measured at room temperature are given in Fig. 4. For the pure P(VDF-HFP) film, the high $\varepsilon_r$ can be attributed to the contribution of the dipoles and mobility of polymer segments above its glass-transition temperature, and the decrease in $\varepsilon_r$ with increasing frequency can be attributed to the fact that the orientation of dipoles can not keep up with the AC field change. In Fig. 4(a), over the entire measured frequency range, the $\varepsilon_r$ of the nanocomposite films increases with the increasing BTO content, which can be easily attributed to the high $\varepsilon_r$ of the BTO filler. It also can be observed that the $\varepsilon_r$ of all the P(VDF-HFP)-BTO films decreases with increasing frequency. Compared with the $\varepsilon_r$ measured at 100 Hz [$\varepsilon_{r(100Hz)}$], the ratios of the changes in $\varepsilon_r$ at different frequencies ($\Delta\varepsilon_r$) to the $\varepsilon_{r(100Hz)}$ are given in Fig. 4(b), where the $\Delta\varepsilon_r = \varepsilon_{r(100Hz)} - \varepsilon_{r(f)}$. It can be observed that the above ratio is weakly affected by the BTO content in the low frequency range, while it obviously decreases with increasing BTO content in the high frequency range. This is due to the weak frequency dependence of $\varepsilon_r$ of BTO and the composition change, and also indicates that the nanocomposite films with high BTO content can exhibit better frequency stability of $\varepsilon_r$. That is, the frequency dependence of the dielectric responses obtained in the composite films is mainly determined the polymer matrix.

In Fig. 4(c), compared with the pure P(VDF-HFP) film, the tan$\delta$ of all the P(VDF-HFP)-BTO films remains at a low value. The tan$\delta$ of all the films slightly decreases with frequency in the range from 100 Hz to about 2 kHz. This phenomenon has been explained by a relaxation process associated with the polymer matrix from the low frequency side rather than the conductivity [45]. It can be seen that in the frequency range from about 2 kHz to 1 MHz, the tan$\delta$ significantly increases with increasing frequency, which has been well studied and attributed the glass-transition process of the polymer matrix, i.e. the motion of the polymer segments. It also can be observed that the tan$\delta$ decreases with increasing BTO content in the high frequency range, which is caused by the composition change and the low dielectric loss of BTO.

The AC conductivity ($\sigma_{ac}$) was calculated using the formula $\sigma_{ac} = 2\pi f\varepsilon_0\varepsilon_r \tan\delta$ [77], where $\varepsilon_0$ ($\varepsilon_0 = 8.85 \times 10^{-12}$ F/m) is the permittivity of the free space, $f$ is the frequency, respectively. The calculated $\sigma_{ac}$ of the P(VDF-HFP)-BTO films are given in Fig. 4(d). The $\sigma_{ac}$ of all the films is quite low and is strongly dependent on frequency, which indicates that they are good insulators. Additionally, the curvature of the AC conductivity spectra is related to the relaxations of the polymer matrix, which has been discussed in our previous work [46]. It also can be seen that the $\sigma_{ac}$ increases with increasing BTO content. This has been attributed to the increase in $\varepsilon_r$ [46], as described by the above formula. To clearly show the influences of BTO content on the $\varepsilon_r$, tan$\delta$, and $\sigma_{ac}$, the data were extracted from Fig. 4 and summarized in Fig. 5.

In order to study influences of the BTO content on the temperature dependences of the dielectric properties of the P(VDF-HFP)-BTO films, the $\varepsilon_r$ and tan$\delta$ were measured in a temperature range from -80 °C to 160 °C at five frequencies (100 Hz, 1 kHz, 10 kHz, 100 kHz and 1 MHz). As shown in Fig. 6(a), there are four processes could be recognized for the pure P(VDF-HFP) film: the α process is associated with the segmental motion in the amorphous regions, i.e. the glass-transition process [70,78–82]; the β process is attributed to the dipolar relaxations of the imperfection in the crystalline regions of the polymer [78], or is associated with the relaxation within the crystalline phase [70,79–82]. The γ process is related to the recrystallization of the polymer. The δ process is observed at quite high temperatures and is significant at low frequencies, which has been attributed to conductivity [83], interfacial polarization [82,84,85], motion of entire polymer chains [44–46]. The

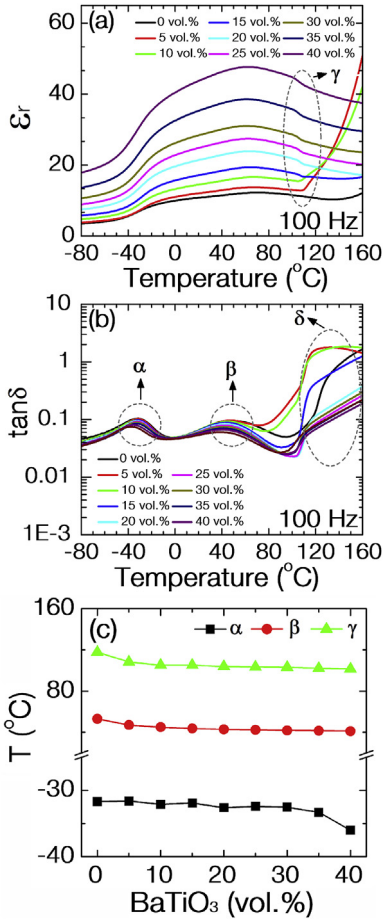


**Fig. 7.** The (a) $\varepsilon_r$ and (b) tan$\delta$ at 100 Hz as a function of temperature of the P(VDF-HFP)-BTO nanocomposite films. (c) The characteristic temperatures of with the α, β and γ processes as a function of BTO content.

temperature dependences of the $\varepsilon_r$ and tan$\delta$ obtained in all composite films are shown in Fig. 6(b)-(i). Clearly, one can find that the temperature dependences of the dielectric properties of all the composite films are similar with that of the pure P(VDF-HFP) film. That is, the temperature dependences of the dielectric properties obtained in the composite films are mainly determined by the polymer matrix.

To identify the influences of the BTO content on these four processes of the polymer matrix, the $\varepsilon_r$ and tan$\delta$ measured at 100 Hz are plotted together, as shown in Fig. 7. In Fig. 7(b), the peaks of the α and β processes are obvious, so that the peak temperatures are used as characteristic values in the flowing discussion. There are no clear phenomena of the γ process in Fig. 7(b) while the γ process can be clearly identified in Fig. 7(a), so that the temperature of the inflection point in Fig. 7(a) is used as the characteristic value of the γ process. It can be seen in Fig. 7(c) that the characteristic temperatures of the α, β and γ processes defined above decrease with increasing BTO content. For the α process, the peak temperature of tan$\delta$ is -31.7 °C for the pure P(VDF-HFP) film, while it is -36.0 °C for the P(VDF-HFP)-*40*BTO film. This indicates that the glass-transition temperature ($T_g$) decreases with increasing BTO content, which has been explained by the interfacial layer between the filler particles and polymer matrix. In the interfacial layer, polymer may have different chain structures, which are dependent on the interaction between the polymer matrix and the surface of the filler particles. And, a weak interaction is necessary for the reduction in the $T_g$ [86–90]. For the β process, the characteristic temperature is 53.1 °C and 41.2 °C for the pure P(VDF-HFP) film and the P(VDF-HFP)-*40*BTO film respectively. This can be attributed to the variation of the mobility of the dipoles with increasing BTO content, and also indicates that the crystallinity of the P(VDF-HFP) in the nanocomposite films is affected by the filler nanoparticles. It is hard to understand that the filler nanoparticles have directly influences on the crystalline regions of the polymer matrix. That is, it is highly possible that the β process is related to the interphase between the crystal regions and the amorphous regions, which may also indicate the imperfection of crystallization as discussed in Fig. 3. For all the nanocomposite films even with 40 vol% of BTO, the β process is obvious. This indicates that though the crystallinity of the P(VDF-HFP) matrix decreases with increasing BTO content, the P(VDF-HFP) in the nanocomposite films still

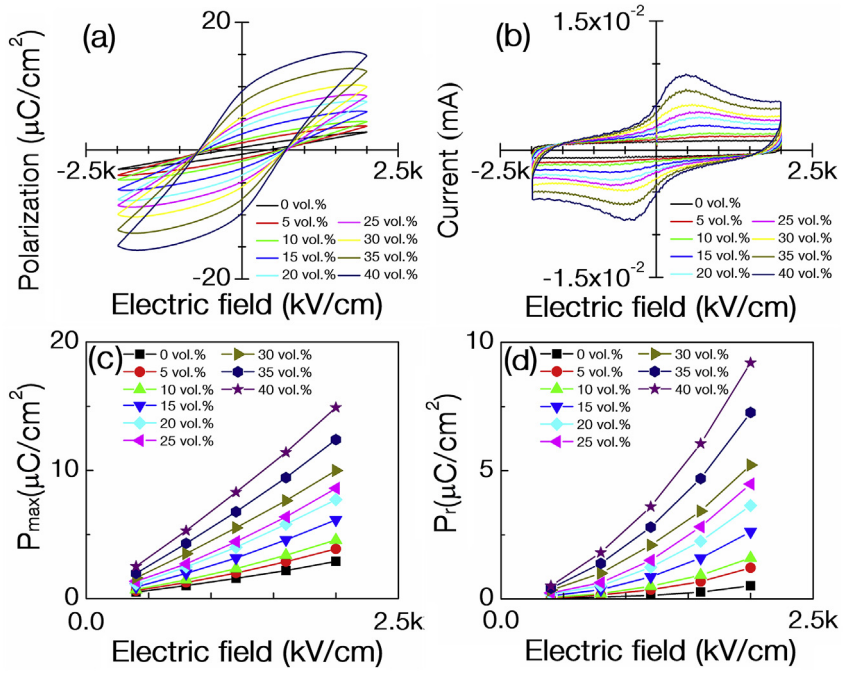


**Fig. 8.** (a) Polarization-electric field (*P*-E) hysteresis loops and (b) the corresponding current-electric field (I-E) curves measured at 100 Hz and at room temperature for the P(VDF-HFP)-BTO nanocomposite films; (c) $P_{max}$ and (d) $P_r$ vs E for the P(VDF-HFP)-BTO nanocomposite films.

is semi-crystalline even with a high filler content, which is in accordance with the discussions in Fig. 3(c). The characteristic temperature of the γ process is independent of frequency, which indicates that the γ process is related to a phase transition, i.e. the recrystallization of the P(VDF-HFP) matrix. It also can be seen that the characteristic temperature of the γ process decreases with increasing BTO content, which is due to the decrease in crystallinity and the reduction in the size of the crystals of the P(VDF-HFP) matrix, as has been discussed in Fig. 3(c). For example, the characteristic temperature of the γ process is 118 °C and 101.7 °C for the pure P(VDF-HFP) film and the P(VDF-HFP)-*40*BTO film respectively.

As mentioned above, the δ process has been addressed to different origins: conductivity, interface polarization, and motion of entire polymer chains. It is clear in Figs. 6 and 7 that, compared with the pure P(VDF-HFP) film, the frequency dispersions of the $\varepsilon_r$ and tan$\delta$ are significant for the P(VDF-HFP)-*5*BTO film, and then are restricted in the nanocomposite films with further increasing BTO content. If the δ process origins from the conductivity at high temperatures, it can be explained as that: with a small filler content (5 vol%), the defects in the nanocomposite films significantly increases, which leads to a higher conductivity that contributes to the dielectric responses. With further increasing filler content, due to hindering effects by the filler nanoparticles to the conductivity of the polymer matrix, the ionic conductivity are hindered and trapped in the interfaces and its contribution to the dielectric responses decreases [82]. If the δ process origins from the interface polarization or the motion of entire polymer chains, the dielectric responses at high temperatures can be explained that: the relaxation times of the interface polarization or the motion of entire polymer chains firstly significantly decreases with a small content of filler and then increases with further increasing filler content. Based on the interface polarization in composites, the detail still is not clear and more efforts are needed to explain the dielectric responses, especially at high temperatures. Based on the motion of entire polymer chains, it has been concluded that a small content of filler could release the mobility of the entire polymer chains, while high content of the fillers could restrict the motion of the entire polymer chains [44].

To conclude, from the analysis of the dielectric properties of the P(VDF-HFP)-BTO composite films measured at different frequencies and at different temperatures, it is clear that both the temperature and frequency dependences of the dielectric responses obtained in the polymer-ceramic composites are mainly determined by the polymer matrix and can be affected by the ceramic filler. The influences of ceramic filler on the dielectric responses associated with the glass transition (i.e. α process), interphase between the crystal regions and the amorphous regions of the polymer matrix (i.e. β process), and the recrystallization of the polymer matrix (i.e. γ process) are clear, but not significant. However, the influences on the dielectric responses associated with the high-temperature process (i.e. δ process) are very strong. That is, these results suggest that, to obtain a good temperature stability in the dielectric properties for the polymer-ceramic composites used in the energy-storage devices, it is critical to choose suitable polymers as matrix. It is experimentally found that the stability of dielectric properties at high temperatures of the polymer-ceramic composite films are significantly affected by the content of ceramic filler, and that a good temperature stability and a small frequency dispersion can be obtained in the composite films with high content of ceramic filler. The above results can be used as guideline for the design and fabrication of polymer-ceramic composite films used in energy-storage devices.

Fig. 8 (a)-(b) shows the polarization-electric field (*P-E*) loops and the corresponding current-electric field (*I-E*) curves of the P(VDF-HFP)-BTO films measured at 100 Hz and under 2000 kV/cm. In Fig. 8(a), compared with the pure P(VDF-HFP) film, the polarization significantly increases and the *P-E* loop turns to be more hysteretic with increasing BTO content, which are attributed to the high polarization of the BTO nanoparticles. In Fig. 8(b), the *I-E* curve becomes fatter with increasing BTO content. It also can be seen that there is no detectable current peak for the pure P(VDF-HFP) film, which indicates that there is no obvious domain switching or phase transition. The polarization current peak becomes much clear with increasing BTO content, which is accompanied by the enhanced hysteresis in the *P-E* loop. The maximal polarization ($P_{max}$) and remnant polarization ($P_r$) with increasing electric field ($E$) are summarized in Fig. 8(c)-(d).

## 4. Conclusion

P(VDF-HFP)-BTO films with a dense and uniform microstructure were successfully fabricated by a spin-coating process and have been systemically characterized. All the free-standing nanocomposite films are translucent and very flexible. Based on the DSC and XRD results, it is found that both the crystallinity and the size of crystals of the P(VDF-HFP) matrix decreases with increasing BTO content. At room temperature, the $\varepsilon_r$ increases and tan$\delta$ decreases with increasing BTO content due to the high $\varepsilon_r$ and low tan$\delta$ of BTO filler. It is found that both the temperature and frequency dependences of the dielectric responses obtained in the composite films are mainly determined by the polymer matrix, whose dielectric responses originate from four dielectric processes: α, β, γ, and δ process. The α process is the glass transition process of the amorphous regions of the polymer matrix. The β process is concluded as the relaxation process associated with the interphase between crystalline regions and amorphous regions. The γ process originates from the recrystallization of the polymer matrix and its characteristic temperature decreases with increasing BTO content due to the facts that both the crystallinity and the size of the crystals of the P(VDF-HFP) matrix decrease with increasing BTO content. The δ process appearing at high temperatures is strongly influenced by the BTO content. The nature of the δ-process is still an open question. Further investigations on the δ-process are needed since this process has a strong contribution to the stability of the dielectric properties of the polymer-ceramic composites at high temperatures.

## Acknowledgement

This research was financially supported by a doctoral starting fund of Xi'an University of Technology (No. 101-256211306) and an USDA NIFA Nanotechnology Grant (No. G00009848).

## References

[1] L. Yang, X. Kong, F. Li, H. Hao, Z. Cheng, H. Liu, J. Li, S. Zhang, Perovskite lead-free dielectrics for energy storage applications, Prog. Mater. Sci. 102 (2019) 72–108.
[2] Q. Hu, L. Jin, T. Wang, C. Li, Z. Xing, X. Wei, Dielectric and temperature stable energy storage properties of $0.88BaTiO_3$-$0.12Bi(Mg_{1/2}Ti_{1/2})O_3$ bulk ceramics, J. Alloy. Comp. 640 (2015) 416–420.
[3] X. Lu, Y. Tong, H. Talebinezhad, L. Zhang, Z.-Y. Cheng, Dielectric and energy-storage performance of $Ba_{0.5}Sr_{0.5}TiO_3$-$SiO_2$ ceramic-glass composites, J. Alloy. Comp. 745 (2018) 127–134.
[4] Y. Tian, L. Jin, H. Zhang, Z. Xu, X. Wei, E.D. Politova, S.Y. Stefanovich, N.V. Tarakina, I. Abrahams, H. Yan, High energy density in silver niobate ceramics, J. Mater. Chem. 4 (2016) 17279–17287.
[5] Z. Yang, F. Gao, H. Du, L. Jin, L. Yan, Q. Hu, Y. Yu, S. Qu, X. Wei, Z. Xu, Y. Wang, Grain size engineered lead-free ceramics with both large energy storage density and ultrahigh mechanical properties, Nano Energy 58 (2019) 768–777.
[6] J. Li, F. Li, Z. Xu, S. Zhang, Multilayer lead-free ceramic capacitors with ultrahigh energy density and efficiency, Adv. Mater. 30 (2018) 1802155.
[7] Z. Yang, H. Du, L. Jin, Q. Hu, S. Qu, Z. Yang, Y. Yu, X. Wei, Z. Xu, A new family of sodium niobate-based dielectrics for electrical energy storage applications, J. Eur. Ceram. Soc. 39 (2019) 2899–2907.
[8] M. Rabuffi, G. Picci, Status quo and future prospects for metallized polypropylene energy storage capacitors, IEEE Trans. Plasma Sci. 30 (2002) 1939–1942.
[9] Y. Wang, X. Zhou, Q. Chen, B. Chu, Q.M. Zhang, Recent development of high energy density polymers for dielectric capacitors, IEEE Trans. Dielectr. Electr. Insul. 17 (2010) 1036–1042.
[10] Z.-Y. Cheng, Q.M. Zhang, Dielectric relaxation behavior and its relation to microstructure in relaxor ferroelectric polymers: high-energy electron irradiated poly (vinylidene fluoride–trifluoroethylene) copolymers, J. Appl. Phys. 92 (2002) 6749–6755.
[11] Z. Li, Y. Wang, Z.-Y. Cheng, Electromechanical properties of poly(inylidene-

fluoride-chlorotrifluoroethylene) copolymer, Appl. Phys. Lett. 88 (2006) 062904.
[12] X. Zhou, S. Zhang, Z. Suo, C. Zou, J. Runt, S. Liu, S. Zhang, Q.M. Zhang, Electrical breakdown and ultrahigh electrical energy density in poly(vinylidene fluoride-hexafluoropropylene) copolymer, Appl. Phys. Lett. 94 (2009) 162901.
[13] B. Chu, X. Zhou, B. Neese, Q.M. Zhang, F. Bauer, Relaxor ferroelectric poly(vinylidene fluoridetrifluoroethylene-chlorofluoroethylene) terpolymer for high energy density capacitors, IEEE Trans. Dielectr. Electr. Insul. 13 (2006) 1162–1169.
[14] B. Chu, X. Zhou, K. Ren, B. Neese, M. Lin, Q. Wang, F. Bauer, Q.M. Zhang, A dielectric polymer with high electric energy density and fast discharge speed, Science 313 (2006) 334–336.
[15] L. Zhu, Q. Wang, Novel ferroelectric polymers for high energy density and low loss dielectrics, Macromolecules 45 (2012) 2937–2954.
[16] W. Xia, Z. Zhang, PVDF-based dielectric polymers and their applications in electronic materials, IET Nanodielectr. 1 (2018) 17–31.
[17] Y. Bai, Z.-Y. Cheng, V. Bharti, H.S. Xu, Q.M. Zhang, High-dielectric-constant ceramic-powder polymer composites, Appl. Phys. Lett. 76 (2000) 3804–3806.
[18] M. Arbatti, X. Shan, Z.-Y. Cheng, Polymer-ceramic composites with high dielectric constant, Adv. Mater. 19 (2007) 1369–1372.
[19] Q. Wang, L. Zhu, Polymer nanocomposites for electrical energy storage, J. Polym. Sci., Part B: Polym. Phys. 49 (2011) 1421–1429.
[20] L. Zhang, Z.-Y. Cheng, Development of polymer-based 0-3 composites with high dielectric constant, J. Adv. Dielectr. 1 (2011) 389–406.
[21] Y. Kobayashi, T. Tanase, T. Tabata, T. Miwa, M. Konno, Fabrication and dielectric properties of the $BaTiO_3$-polymer nano-composite thin films, J. Eur. Ceram. Soc. 28 (2008) 117–122.
[22] Y. Song, Y. Shen, H. Liu, Y. Li, M. Li, C. Nan, Improving the dielectric constants and breakdown strength of polymer composites: effects of the shape of the $BaTiO_3$ nanoinclusions, surface modification and polymer matrix, J. Mater. Chem. 22 (2012) 16491–16498.
[23] J. Zha, Z. Dang, T. Yang, T. Zhou, H. Song, S. Li, Advanced dielectric properties of $BaTiO_3$/Polyvinylidene-fluoride nanocomposites with sandwich multi-layer structure, IEEE Trans. Dielectr. Electr. Insul. 19 (2012) 1312–1317.
[24] X. Zhang, Y. Shen, B. Xu, Q. Zhang, L. Gu, J. Jiang, J. Ma, Y. Lin, C. Nan, Giant energy density and improved discharge efficiency of solution-processed polymer nanocomposites for dielectric energy storage, Adv. Mater. 28 (2016) 2055–2061.
[25] Y. Hao, X. Wang, K. Bia, J. Zhang, Y. Huang, L. Wu, P. Zhao, K. Xu, M. Lei, L. Li, Significantly enhanced energy storage performance promoted by ultimate sized ferroelectric $BaTiO_3$ fillers in nanocomposite films, Nano Energy 31 (2017) 49–56.
[26] Z. Dang, T. Zhou, S. Yao, J. Yuan, J. Zha, H. Song, J. Li, W. Yang, J. Bai, Advanced calcium copper titanate/polyimide functional hybrid films with high dielectric permittivity, Adv. Mater. 21 (2009) 2077–2082.
[27] P. Thomas, S. Satapathy, K. Dwarakanath, K. Varma, Dielectric properties of poly(vinylidene fluoride)/$CaCu_3Ti_4O_{12}$ nanocrystal composite thick films, Express, Polym. Lett. 4 (2010) 632–643.
[28] W. Yang, S. Yu, R. Sun, R. Du, Nano- and microsize effect of CCTO fillers on the dielectric behavior of CCTO/PVDF composites, Acta Mater. 59 (2011) 5593–5602.
[29] L. Zhang, X. Shan, P. Wu, Z.-Y. Cheng, Dielectric characteristics of $CaCu_3Ti_4O_{12}$/P(VDF-TrFE) nanocomposites, Appl. Phys. A 107 (2012) 597–602.
[30] Y. Yang, B.P. Zhu, Z.H. Lu, Z. Wang, C.L. Fei, D. Yin, R. Xiong, J. Shi, Q.G. Chi, Q.Q. Lei, Polyimide/nanosized $CaCu_3Ti_4O_{12}$ functional hybrid films with high dielectric permittivity, Appl. Phys. Lett. 102 (2013) 042904.
[31] L. Zhang, P. Wu, Y. Li, Z.-Y. Cheng, J.C. Brewer, Preparation process and dielectric properties of $Ba_{0.5}Sr_{0.5}TiO_3$-P(VDF-CTFE) nanocomposites, Compos. B Eng. 56 (2014) 284–289.
[32] G. Hu, F. Gao, J. Kong, S. Yang, Q. Zhang, Z. Liu, Y. Zhang, H. Sun, Preparation and dielectric properties of poly(vinylidene fluoride)/$Ba_{0.6}Sr_{0.4}TiO_3$ composites, J. Alloy. Comp. 619 (2015) 686–692.
[33] P. Wu, L. Zhang, X. Shan, Microstructure and dielectric response of $BaSrTiO_3$/P(VDF-CTFE) nanocomposites, Mater. Lett. 159 (2015) 72–75.
[34] Y. Lu, S. Yu, X. Zeng, Rong Sun, C. Wong, High energy density polymer nanocomposites with Y-doped barium strontium titanate nanoparticles as fillers, IET Nanodielectr. 1 (2018) 137–142.
[35] Z. Dang, J. Yuan, J. Zha, T. Zhou, S. Li, G. Hu, Fundamentals, processes and applications of high-permittivity polymer-matrix composites, Prog. Mater. Sci. 57 (2012) 660–723.
[36] Parteek, V.K. Thakur, R.K. Gupta, Recent progress on ferroelectric polymer-based nanocomposites for high energy density capacitors: synthesis, dielectric properties, and future aspects, Chem. Rev. 116 (2016) 4260–4317.
[37] X. Zhang, J. Jiang, Z. Shen, Z. Dang, M. Li, Y. Lin, C. Nan, L. Chen, Y. Shen, Polymer nanocomposites with ultrahigh energy density and high discharge efficiency by modulating their nanostructures in three dimensions, Adv. Mater. 30 (2018) 1707269.
[38] J. Hu, L. Zhang, Z.M. Dang, D. Wang, Improved dielectric properties of polypropylene-based nanocomposites via co-filling with zinc oxide and barium titanate, Compos. Sci. Technol. 148 (2017) 20–26.
[39] J.W. Zha, Q. Cheng, H.D. Yan, W.K. Li, Z.M. Dang, Effect of multi-structured zinc oxide on the electrical properties of polypropylene insulating materials, J. Phys. D Appl. Phys. 50 (2017).
[40] M.S. Zheng, Y.T. Zheng, J.W. Zha, Y. Yang, P. Han, Y.Q. Wen, Z.M. Dang, Improved dielectric, tensile and energy storage properties of surface rubberized $BaTiO_3$/polypropylene nanocomposites, Nano Energy 48 (2018) 144–151.
[41] X. Shan, L. Zhang, X. Yang, Z.-Y. Cheng, Dielectric composites with a high and temperature-independent dielectric constant, J. Adv. Ceram. 1 (2012) 310–316.
[42] L. Zhang, X. Shan, P. Bass, Y. Tong, T.D. Rolin, C.W. Hill, J.C. Brewer, D.S. Tucker, Z.-Y. Cheng, Process and microstructure to achieve ultra-high dielectric constant in polymer-ceramic composites, Sci. Rep. 6 (2016) 35763.
[43] L. Wang, F. Gao, K. Zhang, M. Wang, M. Qin, J. Kong, Effect of hot pressing temperature on dielectric and energy storage properties of $Ba_{0.6}Sr_{0.4}TiO_3$/poly(vinylidene fluoride) Composites, IEEE Trans. Dielectr. Electr. Insul. 24 (2017) 704–711.
[44] X. Lu, Y. Tong, Z.-Y. Cheng, Fabrication and characterization of free-standing, flexible and translucent $BaTiO_3$-P(VDF-CTFE) nanocomposite films, J. Alloy. Comp. 770 (2019) 327–334.
[45] X. Lu, L. Zhang, Y. Tong, Z.-Y. Cheng, BST-P(VDF-CTFE) nanocomposite films with high dielectric constant, low dielectric loss, and high energy-storage density, Compos. B Eng. 168 (2019) 34–43.
[46] X. Lu, Jialiang Shen, L. Zhang, Z. Xu, Z.-Y. Cheng, Dielectric property and ac conductivity of P(VDF-CTFE)-PLZST polymer-ceramic composite films, Ceram. Int. 45 (2019) 8979–8987.
[47] Y. Song, Y. Shen, P. Hu, Y. Lin, C. Nan, Significant enhancement in energy density of polymer composites induced by dopamine-modified $Ba_{0.6}Sr_{0.4}TiO_3$ nanofibers, Appl. Phys. Lett. 101 (2012) 152904.
[48] P. Hu, Y. Song, H. Liu, Y. Shen, Largely enhanced energy density in flexible P (VDF-TrFE) nanocomposites by surface-modified electrospun $BaSrTiO_3$ fibers, J. Mater. Chem. 1 (2013) 1688–1693.
[49] H. Tang, H.A. Sodano, Ultra high energy density nanocomposite capacitors with fast discharge using $Ba_{0.2}Sr_{0.8}TiO_3$ nanowires, Nano Lett. 13 (2013) 1373–1379.
[50] Y. Feng, W.L. Li, Y.F. Hou, Y. Yu, W.P. Cao, T.D. Zhang, W.D. Fei, Enhanced dielectric properties of PVDF-HFP/$BaTiO_3$-nanowires composites induced by interfacial polarization and wire-shape, J. Mater. Chem. C 3 (2013) 1250–1260.
[51] S. Liu, S. Xue, W. Zhang, J. Zhai, Enhanced dielectric an energy storage density induced by surface-modified $BaTiO_3$ nanofibers in poly(vinylidene fluoride) nanocomposites, Ceram. Int. 40 (2014) 15633–15640.
[52] X. Zhang, Y. Shen, Q. Zhang, L. Gu, Y. Hu, J. Du, Y. Lin, C. Nan, Ultrahigh energy density of polymer nanocomposites containing $BaTiO_3$@$TiO_2$ nanofibers by atomic-scale interface engineering, Adv. Mater. 27 (2015) 819–824.
[53] Z. Pan, L. Yao, J. Zhai, S. Liu, K. Yang, H. Wang, J. Liu, Fast discharge and high energy density of nanocomposite capacitors using $Ba_{0.6}Sr_{0.4}TiO_3$ nanofibers, Ceram. Int. 42 (2016) 14667–14674.
[54] Z. Pan, L. Yao, J. Zhai, B. Shen, S. Liu, H. Wang, J. Liu, Excellent energy density of polymer nanocomposites containing $BaTiO_3$@$Al_2O_3$ nanofibers induced by moderate interfacial area, J. Mater. Chem. 4 (2016) 13259–13264.
[55] S. Liu, J. Wang, J. Wang, B. Shen, J. Zhai, C. Guo, J. Zhou, Core-shell structured $BaTiO_3$@$SiO_2$ nanofibers for poly(vinylidene fluoride) nanocomposites with high discharged energy, Mater. Lett. 189 (2017) 176–179.
[56] M. Rahimabady, M.S. Mirshekarloo, K. Yao, L. Lu, Dielectric behaviors and high energy storage density of nanocomposites with core-shell $BaTiO_3$@$TiO_2$ in poly (vinylidene fluoride-hexafluoropropylene), Phys. Chem. Chem. Phys. 15 (2013) 16242–16248.
[57] K. Bi, M. Bi, Y. Hao, W. Luo, Z. Cai, X. Wang, Y. Huang, Ultrafine core-shell BaTiO3@$SiO_2$ structures for nanocomposite capacitors with high energy density, Nano Energy 51 (2018) 513–523.
[58] Q. Zhang, Y. Jiang, E. Yu, H. Yang, Significantly enhanced dielectric properties of P(VDF-HFP) composite films filled with core-shell BaTiO3@PANI nanoparticles, Surf. Coating. Technol. 358 (2019) 293–298.
[59] M. Zhu, X. Huang, K. Yang, X. Zhai, J. Zhang, J. He, P. Jiang, Energy storage in ferroelectric polymer nanocomposites filled with core-shell structured polymer@$BaTiO_3$ nanoparticles: understanding the role of polymer shells in the interfacial regions, ACS Appl. Mater. Interfaces 6 (2014) 19644–19654.
[60] X. Huang, P. Jiang, Core-shell structured high-k polymer nanocomposites for energy storage and dielectric applications, Adv. Mater. 27 (2015) 546–554.
[61] X. Zhang, S. Zhao, F. Wang, Y. Ma, L. Wang, D. Chen, et al., Improving dielectric properties of $BaTiO_3$/poly(vinylidene fluoride) composites by employing core-shell structured $BaTiO_3$@Poly(methylmethacrylate) and $BaTiO_3$@Poly(trifluoroethyl methacrylate) nanoparticles, Appl. Surf. Sci. 403 (2017) 71–79.
[62] S. Liu, J. Wang, H. Hao, L. Zhao, J. Zhai, Discharged energy density and efficiency of nanocomposites based on poly (vinylidene fluoride) and core-shell structured $BaTiO_3$@$Al_2O_3$ nanoparticles, Ceram. Int. 44 (2018) 22850–22855.
[63] T. Zhou, J. Zha, R. Cui, B. Fan, J. Yuan, Z. Dang, Improving dielectric properties of $BaTiO_3$/ferroelectric polymer composites by employing surface hydroxylated $BaTiO_3$ nanoparticles, ACS Appl. Mater. Interfaces 3 (2011) 2184–2188.
[64] Z.H. Dai, T. Li, Y. Gao, J. Xu, J. He, Y. Weng, B.H. Guo, Achieving high dielectric permittivity, high breakdown strength and high efficiency by cross-linking of poly (vinylidene fluoride)/BaTiO3 nanocomposites, Compos. Sci. Technol. 169 (2019) 142–150.
[65] S. Liu, S. Xue, W. Zhang, J. Zhai, G. Chen, Significantly enhanced dielectric property in PVDF nanocomposites flexible films through a small loading of surface-hydroxylated $Ba_{0.6}Sr_{0.4}TiO_3$ nanotubes, J. Mater. Chem. 2 (2014) 18040–18046.
[66] S. Liu, S. Xue, S. Xiu, B. Shen, J. Zhai, Surface-modified Ba $(Zr_{0.3}Ti_{0.7})O_3$ nanofibers by polyvinylpyrrolidone filler for poly (vinylidene fluoride) composites with enhanced dielectric constant and energy storage density, Sci. Rep. 6 (2016) 26198.
[67] Y. Tong, L. Zhang, P. Bass, T.D. Rolin, Z.-Y. Cheng, Influence of silane coupling agent on microstructure and properties of CCTO-P(VDF-CTFE) composites, J. Adv. Dielect. 8 (2018) 1850008.
[68] P. Hu, S. Gao, Y. Zhang, L. Zhang, C. Wang, Surface modified BaTiO3 nanoparticles by titanate coupling agent induce significantly enhanced breakdown strength and larger energy density in PVDF nanocomposite, Compos. Sci. Technol. 156 (2018) 109–116.
[69] Z. Li, F. Liu, G. Yang, L. Ren, L. Dong, C. Xiong, Q. Wang, Enhanced energy storage performance of ferroelectric polymer nanocomposites at relatively low electric fields induced by surface modified $BaTiO_3$ nanofibers, Compos. Sci. Technol. 164 (2018) 214–221.
[70] P. Frübing, F. Wang, M. Wegener, Relaxation processes and structural transitions in

stretched films of polyvinylidene fluoride and its copolymer with hexafluoropropylene, Appl. Phys. A 107 (2012) 603–611.
[71] C. Ehrhardt, C. Fettkenhauer, J. Glenneberg, W. Munchgesang, H.S. Leipner, G. Wagner, M. Diestelhorst, C. Pientschke, H. Beige, S.G. Ebbinghaus, Enhanced dielectric properties of sol-gel-$BaTiO_3$/P(VDF-HFP) composite films without surface functionalization, RSC Adv. 4 (2014) 40321–40329.
[72] J. Liu, X.L. Lu, C.R. Wu, Effect of annealing conditions on crystallization behavior and mechanical properties of NIPS poly(vinylidene fluoride) hollow fiber membranes, J. Appl. Polym. Sci. 129 (2013) 1417–1425.
[73] J. Jiang, X. Zhang, Z. Dan, J. Ma, Y. Lin, M. Lin, C.W. Nan, Y. Shen, Tuning phase composition of polymer nanocomposites towards high energy density and high discharge efficiency by non-equilibrium processing, ACS Appl. Mater. Interfaces 9 (2017) 29717–29731.
[74] K.M. Kim, N.G. Park, K.S. Ryu, S.H. Chang, Characteristics of PVdF-HFP/$TiO_2$ composite membrane electrolytes prepared by phase inversion and conventional casting methods, Electrochim. Acta 51 (2006) 5636–5644.
[75] K. Prabakaran, S. Mohanty, S.K. Nayak, Influence of surface modified $TiO_2$ nanoparticles on dielectric properties of PVdF-HFP nanocomposites, J. Mater. Sci. Mater. Electron. 25 (2014) 4590–4602.
[76] C. Merlini, G.M.O. Barra, T. Medeiros Araujo, A. Pegoretti, Electrically pressure sensitive poly(vinylidene fluoride)/polypyrrole electrospun mats, RSC Adv. 4 (2014) 15749–15758.
[77] X. Yao, L. Zhang, Dielectric Physics (Chinese), Xi'an Jiaotong University Press, Xi'an, 1991, pp. 339–340.
[78] M. Li, H.J. Wondergem, M.J. Spijkman, K. Asadi, I. Katsouras, P.W.M. Blom, D.M. Leeuw, Revisiting the δ-phase of poly(vinylidene fluoride) for solution-processed ferroelectric thin films, Nat. Mater. 12 (2018) 433–441.
[79] V. Valentin, Kochervinskii, I. Malyshkina, G.V. Markin, N.D. Gavrilova, N.P. Bessonova, Dielectric relaxation in vinylidene fluoride-hexafluoropropylene copolymers, J. Appl. Polym. Sci. 105 (2007) 1101–1117.
[80] X. Zhao, W. Liu, X. Jiang, K. Liu, G. Peng, Z. Zhan, Exploring the relationship of dielectric relaxation behavior and discharge efficiency of P(VDF-HFP)/PMMA blends by dielectric spectroscopy, Mater. Res. Express 3 (2016) 075304.
[81] J.F. Mano, V. Sencadas, A. Mello Costa, S. Lanceros-Méndez, Dynamic mechanical analysis and creep behaviour of β-PVDF films, Mater. Sci. Eng. A 370 (2004) 336–340.
[82] H. Rekik, Z. Ghallabi, I. Royaud, M. Arous, G. Seytre, G. Boiteux, A. Kallel, Dielectric relaxation behaviour in semi-crystalline polyvinylidene fluoride (PVDF)/$TiO_2$ nanocomposites, Compos. B Eng. 45 (2013) 1199–1206.
[83] V. Tomer, E. Manias, C.A. Randall, High field properties and energy storage in nanocomposite dielectrics of poly(vinylidene fluoride-hexafluoropropylene), J. Appl. Phys. 110 (2011) 044107.
[84] C.V. Chanmal, J.P. Jog, Dielectric relaxations in PVDF/$BaTiO_3$ nanocomposites, Express Polym. Lett. 2 (2008) 294–301.
[85] S.F. Mendes, C.M. Costa, R.S.I. Serra, A.A. Baldalo, V. Sencadas, J.L. Gomez-Ribelles, R. Gregorio, S. Lanceros-Mendez, Influence of filler size and concentration on the low and high temperature dielectric response of poly(vinylidene fluoride)/Pb($Zr_{0.53}Ti_{0.47}$)$O_3$ composites, J. Polym. Res. 19 (2012) 9967.
[86] H. Nguyen, X. Liang, M. Ito, K. Nakajima, Direct mapping of nanoscale viscoelastic dynamics at nanofiller/polymer interfaces, Macromolecules 51 (2018) 6085–6091.
[87] D. Pitsa, M. Danikas, Interfaces features in polymer nanocomposites: a review of proposed models, Nano: Brief Rep. Rev. 6 (2011) 497–508.
[88] F.W. Starr, T.B. Schroder, S.C. Glotzer, Effects of a nanoscopic filler on the structure and dynamics of a simulated polymer melt and the relationship to ultrathin films, Phys. Rev. E: Stat. Phys., Plasmas, Fluids 64 (2001) 021802.
[89] M. Bansal, H. Yang, C. Li, K. Cho, B.C. Benicewicz, S.K. Kumar, L.S. Schadler, Quantitative equivalence between polymer nanocomposites and thin polymer films, Nat. Mater. 4 (2005) 693–698.
[90] F.W. Starr, J.F. Douglas, D. Meng, S.K. Kumar, Bound Layers "cloak" nanoparticles in strongly interacting polymer nanocomposites, ACS Nano 10 (2016) 10960–10965.